



## Tuning the microstructure and mechanical properties of additive manufactured aluminum matrix composites by cold spray

Qiang Wang<sup>a,b,\*</sup>, Wenjuan Niu<sup>b,\*\*</sup>, Xu Li<sup>b</sup>, Peng Han<sup>b</sup>, Xuan Mao<sup>b</sup>, Ju Yang<sup>b</sup>, Ming-Xing Zhang<sup>c</sup>

<sup>a</sup> Shaanxi Key Laboratory of Surface Engineering and Remanufacturing, Xi'an University, Xi'an 710065, China

<sup>b</sup> School of Metallurgical Engineering, Xi'an University of Architecture and Technology, Xi'an 710055, China

<sup>c</sup> Division of Materials, School of Mechanical and Mining Engineering, The University of Queensland, St. Lucia, QLD 4072, Australia



### ARTICLE INFO

**Keywords:**

Cold spraying  
Aluminum matrix composites  
Heat treatment  
Microstructure  
Mechanical properties

### ABSTRACT

Cold spray (CS) has significant technical advantages in additive manufacturing of aluminum matrix composites. In this study, Al with different content of  $\text{Al}_2\text{O}_3$  composite deposits was successfully produced by CS. The effect of  $\text{Al}_2\text{O}_3$  content and heat treatment temperature on the microstructure and mechanical properties of the deposits was comprehensively studied. The results show that as the content of  $\text{Al}_2\text{O}_3$  increases, the hardness, Ultimate Tensile Strength (UTS), and elongation of the deposits gradually improve in the as-sprayed state. Due to the significant hammering effect of  $\text{Al}_2\text{O}_3$  particles on Al particles, there is a local metallurgical bond between adjacent Al particles in Al-50 and Al-75 deposits, and dimples appear in the fracture morphology of the deposit. With the increase of the heat treatment temperature, the diffusion of atoms at the particle-particle interface transforms the bonding between Al particles from mechanical interlocking to metallurgical bonding, so that the deposit exhibits improved ductility. However, heat treatment also eliminates the residual compressive stress and introduces grain growth through recovery and recrystallization processes, resulting in the decrease of hardness and UTS of the deposits.

### 1. Introduction

Aluminum matrix composites (AMCs) have high strength-weight ratio, high stiffness, and enhanced wear resistance, and been widely used in transportation and defense areas [1]. The performance of AMCs is influenced by the properties, content, and distribution of reinforcements, such as SiC, TiC, and  $\text{Al}_2\text{O}_3$  [2–4]. Compared with the conventional preparation methods, including stir casting and powder metallurgy, the additive manufacturing (AM) has the ability to directly produce complex parts, and the manufacturing process & cycle time and energy consumption are greatly reduced.

Cold spray (CS) is an emerging competitive additive manufacturing technique with the unique feature of a complete solid-state forming process [5,6]. In this process, the high-pressure gas ( $\text{N}_2$ , He or Compressed Air) which is heated to temperatures far below the melting point of spraying materials is used to drive the micron-sized powder particles (in the range of 1–50  $\mu\text{m}$ ) to high velocities (300–1200 m/s), and then

the deposition of particles are achieved through severe plastic deformation upon impacting [6–10]. In comparison with the high energy source, such as laser, electron beam, arc and plasma, assisted AM techniques, CS can minimize the thermal defects, such as oxidation, phase transformation, decomposition and grain growth of the raw material [7,9]. In addition, CS deposit retains compressive residual stress and has a high deposition rate, approximately one order of magnitude higher than laser deposition process [4,9]. Based on these advantages, CS can process a wide range of materials, including pure metals, alloys, amorphous materials and metal matrix composites (MMCs) [11–14]. Moreover, CS can produce smaller spray line widths by installing micro-nozzles to improve spray space resolution and control additive manufacturing precision, which makes CS suitable for AM applications [6,9].

The previous studies have revealed that the CS deposited AMC ( $\text{Al}-\text{Al}_2\text{O}_3$ ) coatings have enhanced density, hardness and good wear resistance, owing to the hammering effect of ceramic particles which

\* Correspondence to: Q. Wang, Shaanxi Key Laboratory of Surface Engineering and Remanufacturing and Xi'an University of Architecture and Technology, China.

\*\* Correspondence to: W. Niu, Xi'an University of Architecture and Technology, China.

E-mail addresses: [qiang.wang@xauat.edu.cn](mailto:qiang.wang@xauat.edu.cn) (Q. Wang), [niuwenjuanmm@163.com](mailto:niuwenjuanmm@163.com) (W. Niu).

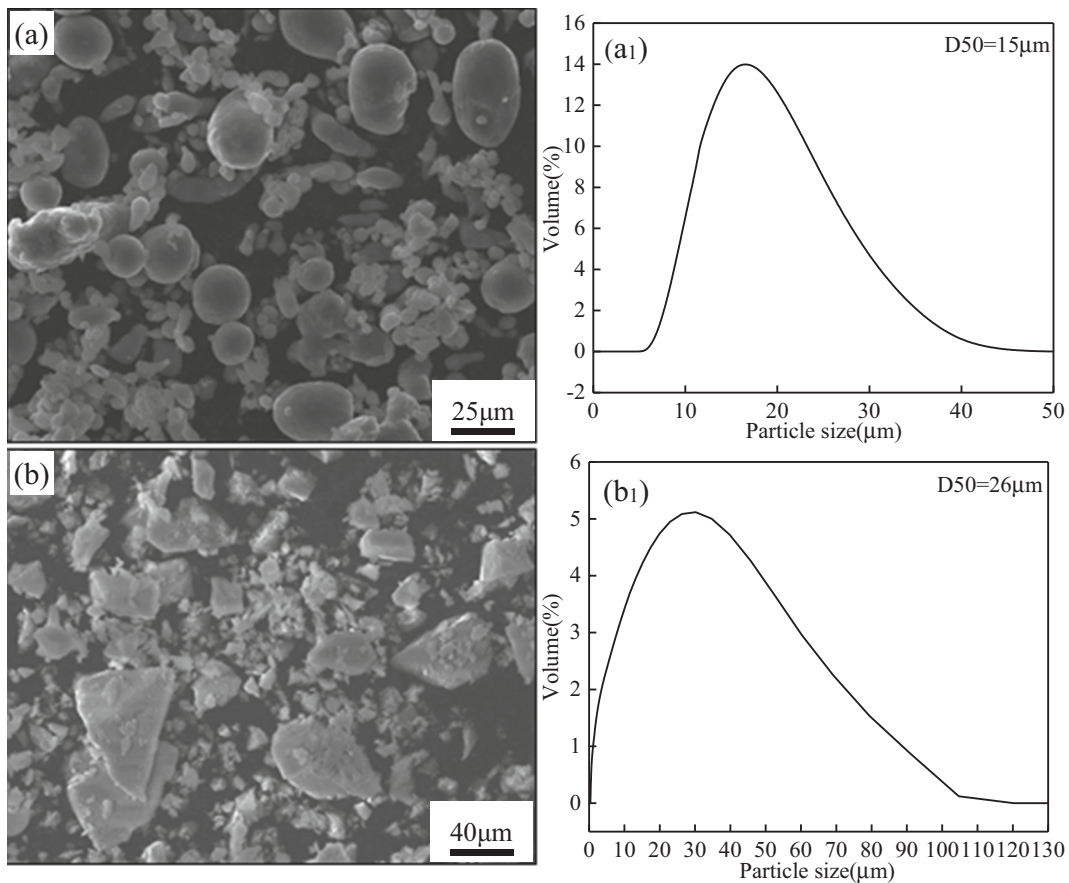


**Fig. 1.** The secondary electron SEM micrographs and particle size distribution of Al powder and Al<sub>2</sub>O<sub>3</sub> powder, (a) and (a') Al powder, (b) and (b') Al<sub>2</sub>O<sub>3</sub> powder.

increased the plastic deformation and the interfacial bonding of Al particles [15–18]. However, the highly restored strain energy resulting from severe plastic deformation leads to the formation of high-density dislocations, particularly located along the particle-particle interface region, which makes CS deposits extremely brittle and tend to rupture [19–22]. Therefore, it is necessary to carry out post heat treatment to improve the ductility and toughness of CS deposits towards the application as bulk materials. In the present study, the effect of heat treatment process and ceramic content on microstructural evolution, hardness, and tensile properties will be symmetrically studied. The bonding and fracture mechanism of CS AMC deposits will be discussed.

## 2. Experimental procedures

### 2.1. Material deposition

The raw material powders used are spherical and ellipsoidal pure Al powder with a size distribution of 5 to 15 μm and irregular α-Al<sub>2</sub>O<sub>3</sub> powder in a range of 5 to 30 μm, as shown in Fig. 1. The powder mixtures of Al with 25, 50, and 75 vol% Al<sub>2</sub>O<sub>3</sub> were mixed in a Turbula mixer for 1 h, followed by vacuum drying at 80 °C for 24 h prior to spraying. The cold spray experiment was carried out by using the low-pressure cold spray system at the Cold Spray Technology R&D Center, Xi'an University

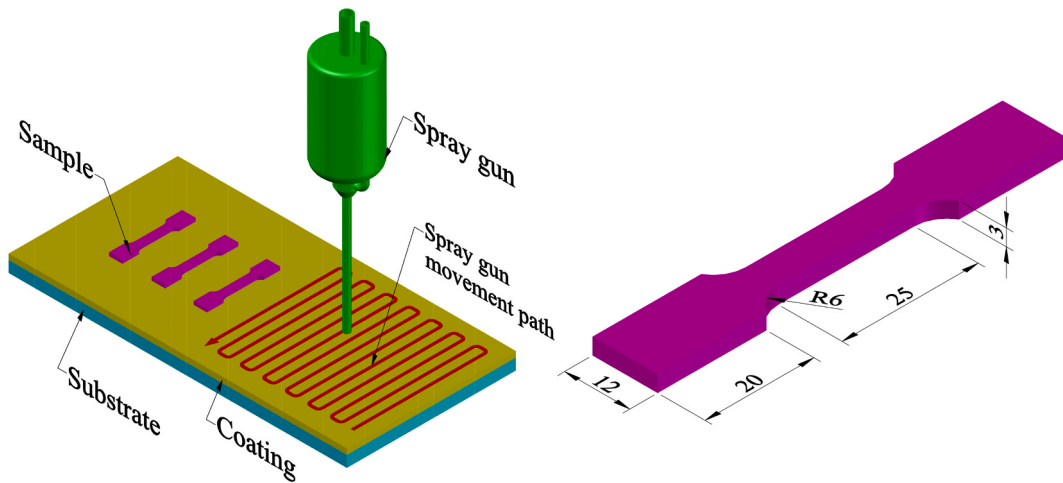


**Fig. 2.** Sampling position and size (mm) of non-standard specimens in tensile test.

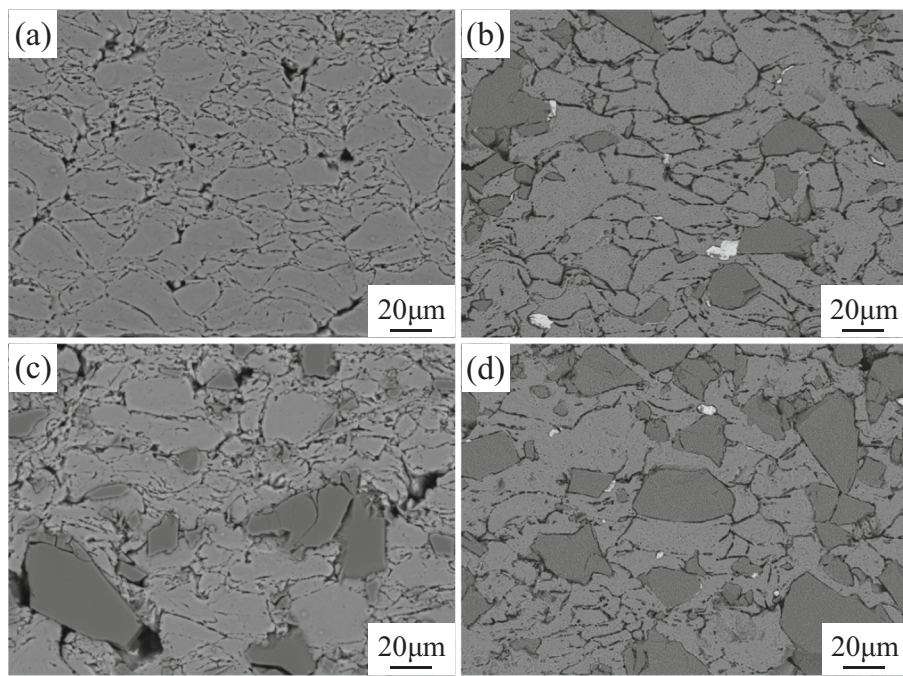


Fig. 3. The cross-sectional microstructure of CS-AM deposits, (a) Al-0, (b) Al-25, (c) Al-50, (d) Al-75.

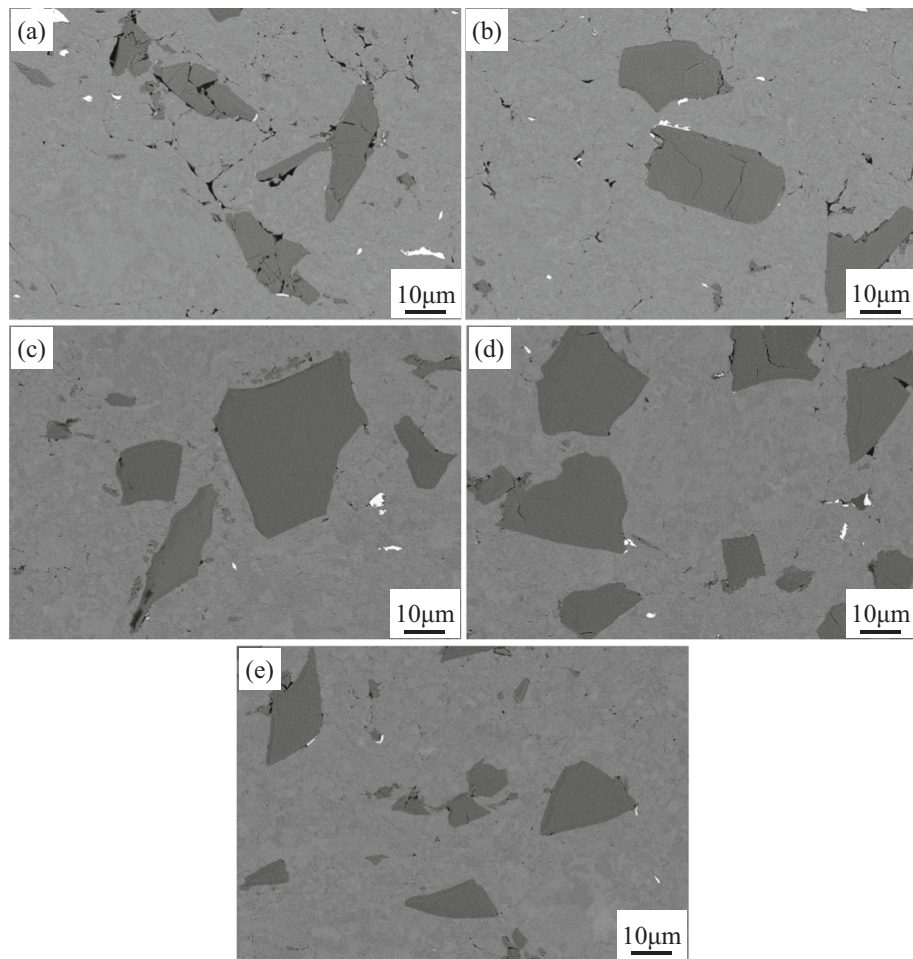
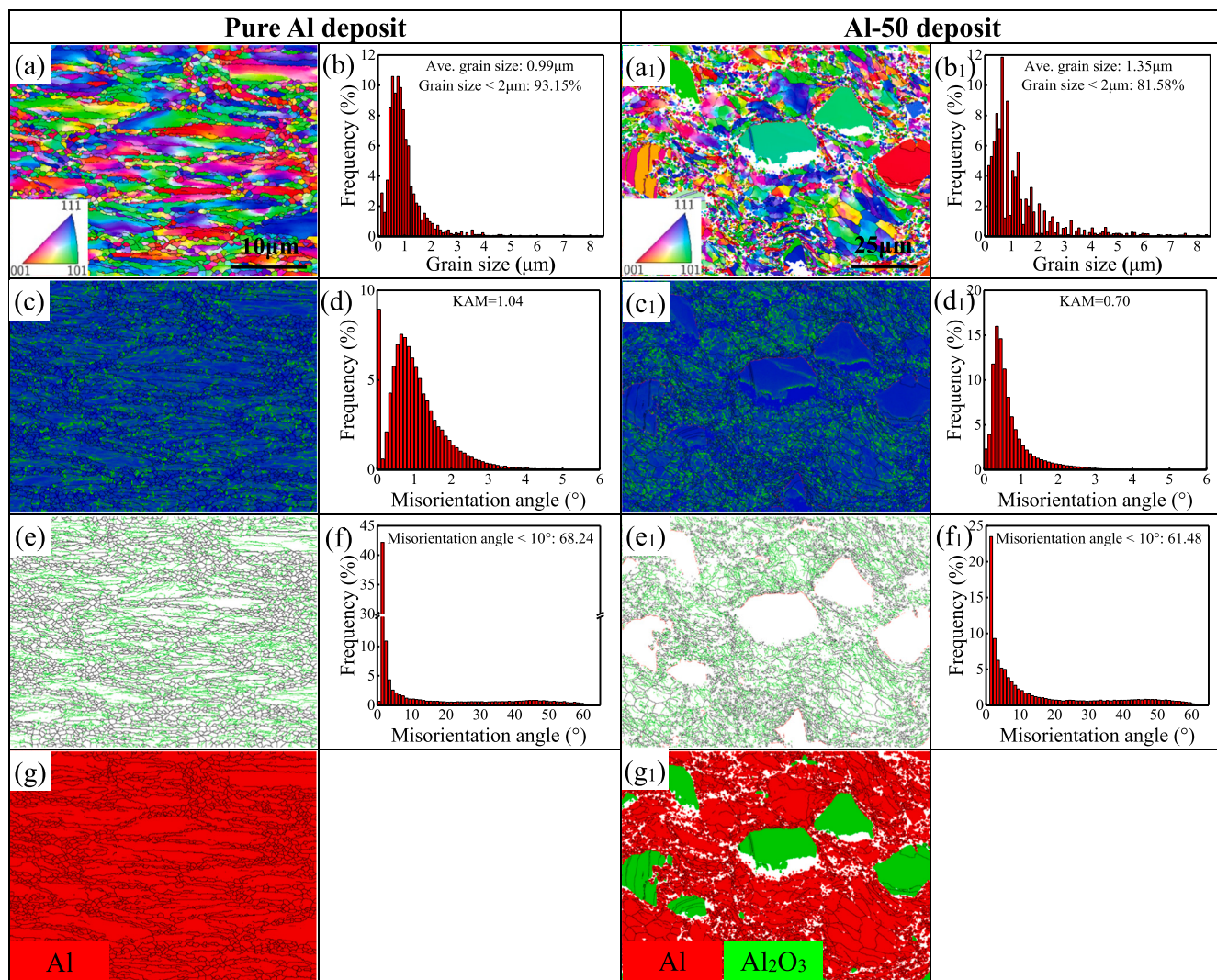


Fig. 4. The cross-sectional microstructure of CS-AM Al-50 deposits, (a) as-sprayed, and heat treated for 2 h at (b) 150 °C, (c) 250 °C, (d) 350 °C, (e) 450 °C and (f) 550 °C.



**Fig. 5.** EBSD characterization of as-sprayed CS-AM Al-0 and Al-50 deposit, (a) and (a<sub>1</sub>) are inverse pole figure (IPF), (b) and (b<sub>1</sub>) are grain size distribution, (c) and (c<sub>1</sub>) are kernel average misorientation (KAM) map, (d) and (d<sub>1</sub>) are KAM map local misorientation bar, (e) and (e<sub>1</sub>) are grain boundary distribution map, (f) and (f<sub>1</sub>) are corresponding misorientation distribution plot shows the statistic of grain boundaries, (g) and (g<sub>1</sub>) are phase distribution map.

of Architecture and Technology. N<sub>2</sub> was used as the driving gas, and the gas pressure and temperature were set at 1.0 MPa and 400 °C, respectively. The spray distance was 12 mm. The pure Al plate was used as the substrate, and the length, width and height of the substrate were 100 mm, 100 mm and 10 mm, respectively. The preparation process of deposits was divided into two steps. The first was to spray the mixed powder on the surface of the substrate, and second step was to cut the deposits from the substrate surface using Wire Electrical Discharge Machining (WEDM) cut, and the samples were labeled as Al-0, Al-25, Al-50 and Al-75 according to the volume ratio of Al<sub>2</sub>O<sub>3</sub> in the mixed powder.

## 2.2. Analysis of coating microstructure and mechanical properties

The deposited materials were heat-treated in a vacuum heat treatment furnace at five temperatures from 150 °C to 550 °C, with an interval of 100 °C. The heating rate was 10 °C/min, and the holding time was 2 h, followed with furnace cooling. The heat-treated materials were labeled as HT150, HT250, HT350, HT450, HT550, respectively. The microstructure of deposits was examined by scanning electron microscopy (SEM, GeminiSEM 300). The porosity of deposits was measured by means of image analysis, and the values were averaged using 10

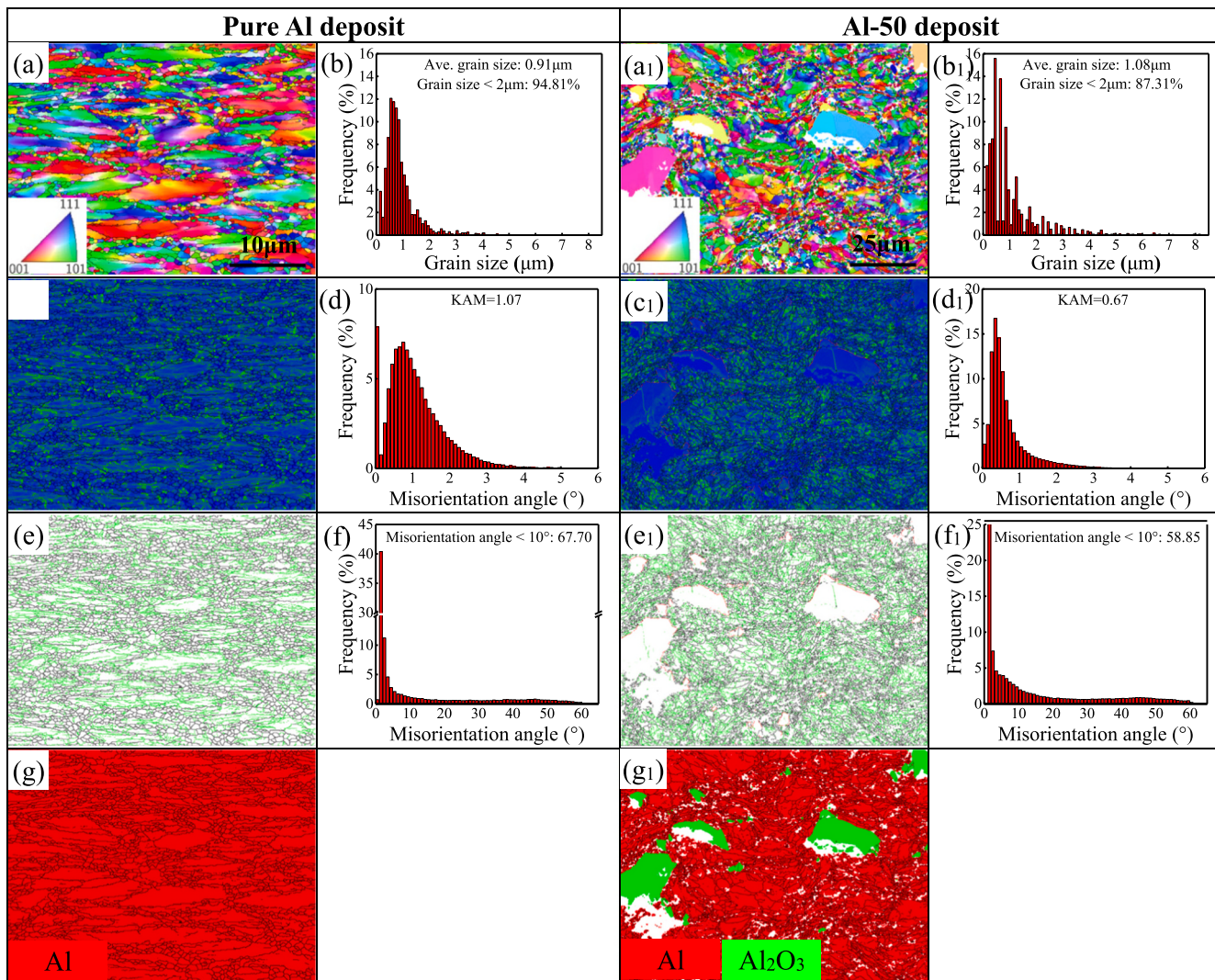
backscatter SEM images captured randomly within the deposits. The electron backscatter diffraction (EBSD) was used to characterize the microstructural evolution of deposits before and after heat treatment.

Fig. 2 shows the sampling position and size of tensile specimens. The tensile test was carried out by the Instron M8801 electro-hydraulic servo machine, and three measurements were done for each deposit at a tensile rate of 0.5 mm/min. The displacement was monitored using a mechanical extensometer during the tensile test. The microhardness test was performed by using a Vickers microhardness tester with a load of 250 g and a duration time of 15 s. The hardness value was taken as the average of 10 measurements for each specimen. The microstructure and fracture morphology of the material were characterized by SEM.

## 3. Results and discussion

### 3.1. Microstructural evolution of the CS-AM deposited materials

Fig. 3 shows the cross-sectional microstructure of as-sprayed deposits, and the porosity was measured to be 0.97%, 0.94%, 1.85%, and 1.81% for Al-0, Al-25, Al-50, Al-75, respectively. The deposits are dense, and the ceramic particles are dispersed uniformly within the composites. However, with the increase of the content of ceramic particles in the



**Fig. 6.** EBSD characterization of CS-AM Al-0 and Al-50 deposit under HT150 conditions, (a) and (a<sub>1</sub>) are inverse pole figure (IPF), (b) and (b<sub>1</sub>) are grain size distribution, (c) and (c<sub>1</sub>) are kernel average misorientation (KAM) map, (d) and (d<sub>1</sub>) are KAM map local misorientation bar, (e) and (e<sub>1</sub>) are grain boundary distribution map, (f) and (f<sub>1</sub>) are corresponding misorientation distribution plot shows the statistic of grain boundaries, (g) and (g<sub>1</sub>) are phase distribution map.

mixed powder, the probability of ceramic particles impacting with each other increases during the powder deposition process, leading to the increase of the porosity of the coating. But during the deposition process, the hammering effect of ceramic particles made the deformation of Al particles more intense and enhanced the interfacial bonding between Al particles, and plays an important role in improving the UTS of the deposit, as explained in 3.2.

Fig. 4 shows the typical SEM microstructure evolution after heat treatment in a range of 150 °C to 550 °C with an interval of 100 °C, in an example of Al-50 deposit, and the porosity of heat-treated samples was measured to be 1.84%, 1.52%, 0.74%, 0.70% and 0.65%, respectively. Compared with as-sprayed deposits, the porosity gradually decreased with increasing heat treatment temperature. The porosity of Al-50-HT350 sample decreased obviously. Similar observations have been made in previous studies, where solid diffusion occurred during the heat treatment of cold sprayed deposit, resulting in densified structures with reduced porosity. [23]. The self-diffusion coefficient of Al at 345 °C is  $5.23 \times 10^{-16}$  (cm<sup>2</sup>/s) as reported by Messer et al. [24]. After 2 h of heat treatment, the theoretical diffusion distance of the aluminum atom is 1.94 μm. Therefore, it can be concluded that heat treatment at 345 °C can seal a pore less than 2 μm, which can explain the effect of annealing treatment on the density of the coating.

The CS process is a cold deformation process of individual metallic particles during the deposition. Therefore, the microstructure of as-sprayed materials generally has a similar representation to that of cold rolled plates, i.e. elongated splats with lamellar structure, which restored high strain energy and residual stresses [25]. This kind of microstructure is responsible for the low ductility. Upon heat treatment, the microstructure of as-sprayed materials will change in three stages, including recovery, recrystallization, and grain growth.

Therefore, in order to quantify the microstructural evolution at various stages, EBSD analysis was conducted on representative sample conditions of as-sprayed, HT150, HT350, and HT550.

Fig. 5 shows the EBSD analysis results of as-sprayed CS-AM Al-0 and Al-50 deposits. Owing to the severe plastic deformation resulting from high velocity impact, particles transformed into splats with relatively coarse grain structure surrounded by clusters of randomly-oriented small grains, as shown by the inverse pole figure (IPF) map in Fig. 5 (a) and (a<sub>1</sub>). The formation of this unique shell-like structure was attributed to the localized deformation which concentrated in regions of particles' surface upon rapid collisions, i.e., most of the impact energy was absorbed by the surface of particles, and the grains in the surface area undergo dynamic recrystallization, thus forming fine grains [26].

The statistical results revealed that the average grain sizes of as-

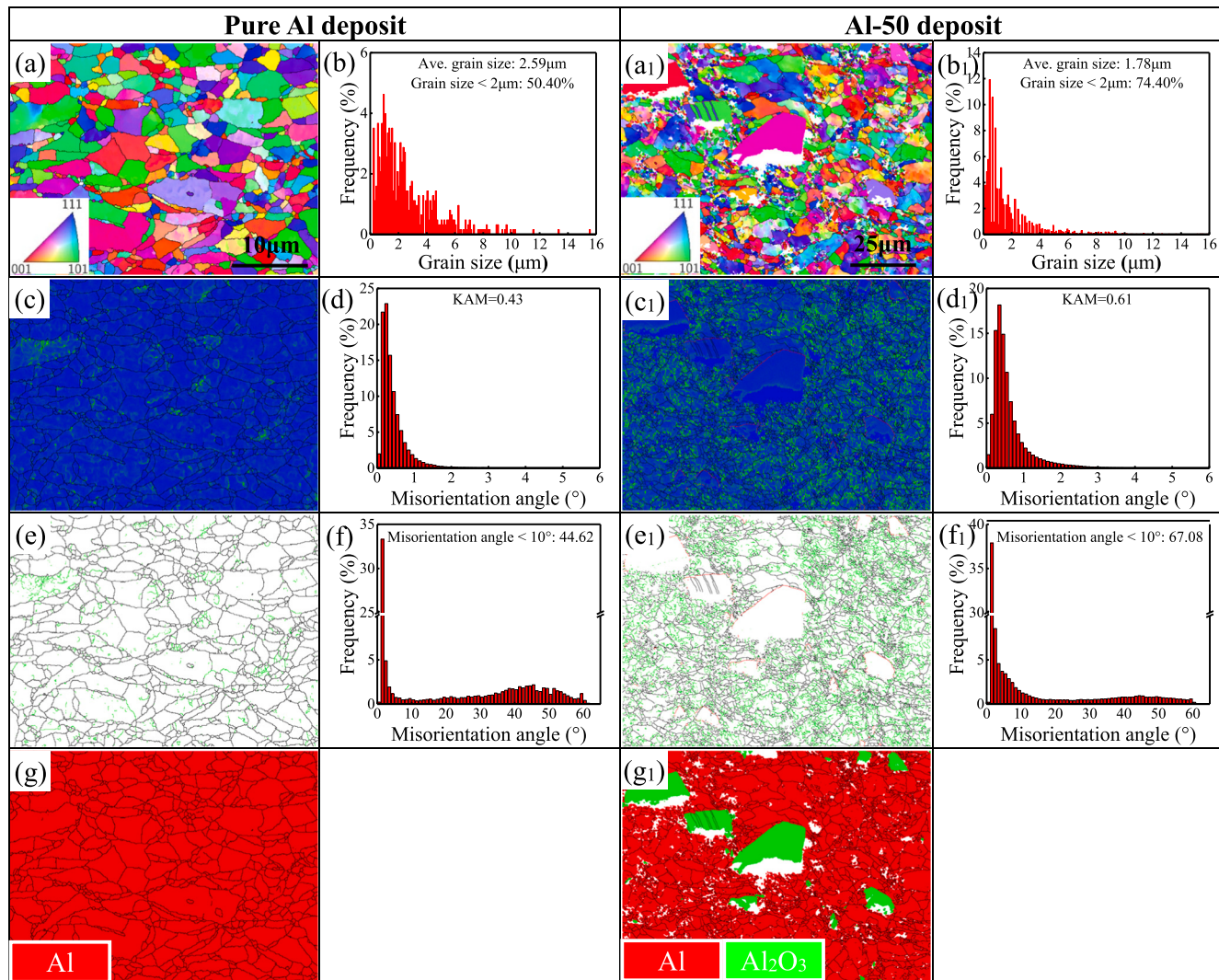


**Fig. 7.** EBSD characterization of CS-AM Al-0 and Al-50 deposit under HT350 conditions, (a) and (a<sub>1</sub>) are inverse pole figure (IPF), (b) and (b<sub>1</sub>) are grain size distribution, (c) and (c<sub>1</sub>) are kernel average misorientation (KAM) map, (d) and (d<sub>1</sub>) are KAM map local misorientation bar, (e) and (e<sub>1</sub>) are grain boundary distribution map, (f) and (f<sub>1</sub>) are corresponding misorientation distribution plot shows the statistic of grain boundaries, (g) and (g<sub>1</sub>) are phase distribution map.

sprayed CS-AM Al-0 and Al-50 are 0.99 μm and 1.35 μm, respectively, as shown in Fig. 5(b) and (b<sub>1</sub>). The formation of such refined grains was attributed to the deformation induced dynamic recrystallization (DRX), i.e., deformation resulted in accumulation of high density of dislocations which stimulated the grain refinement process through crystal rotation [27]. The crystal rotation was evidenced from the color gradient within the relatively coarse grains, as seen in the IPF map (Fig. 5a and a<sub>1</sub>) where the color gradient represented the grain orientation. The kernel average misorientation (KAM) map is used to reflect the strain existing in the grains as an estimate of the dislocation density near the grain boundaries [28]. The statistic of local misorientation within individual grains was given by KAM map in Fig. 5(c) and (c<sub>1</sub>). The coarse grains generally possessed a local misorientation up to 4°. Such crystal rotation generally led to the formation of substructures, which were characterized by the grain boundary distribution map in Fig. 5(e) and (e<sub>1</sub>), grain boundaries between 2 and 10 degrees are in green (low angle grain boundaries, LAGBs) and higher than 10 degrees are in black (high angle grain boundaries, HAGBs). The LAGBs in the Al-0 and Al-50 deposits accounted for 68.24% and 61.48% of the total grain boundary area, respectively, indicating that there are many substructures in the deposits. Therefore, these EBSD analytical results confirmed the inhomogeneous deformation of particles during CS deposition, including refined

small grains and highly distorted coarse grains with large number of substructures. This would deteriorate the ductility of as-sprayed deposit.

We all know that the Al<sub>2</sub>O<sub>3</sub> particles in the deposits can promote the deformation of Al particles through the hammering effect and enhance the mechanical bonding strength between the particles. As shown in Fig. 5(a) and (a<sub>1</sub>), it can be found that the original outline of Al particles can be clearly distinguished in Al-0, while the original outline of Al particles can hardly be distinguished in Al-50. It shows that the deformation of the particles in the Al-50 deposit is indeed more severe. However, in the above analysis, it is found that the proportion of small-sized grains in Al-50, the KAM value, etc. are all smaller than the correlation value in Al-0. The analysis believes that the main reason for this phenomenon is that the grain distortion in the Al-50 deposit is too large, and it is difficult to obtain the information of the severely distorted area during the sample scanning process, which leads to errors in the statistical results (In the experiment, the EBSD image resolution rate of Al-50 was only 72%).

Fig. 6 shows the EBSD analysis results of Al-0 and Al-50 deposits after heat treatment at 150 °C. The statistical results revealed that the average grain sizes of Al-0 and Al-50 are 0.91 μm and 1.08 μm, respectively, as shown in Fig. 6(b) and (b<sub>1</sub>). From the IPF map (Fig. 6a & a<sub>1</sub>), the grain distribution and morphology of the deposits show a similar phenomenon

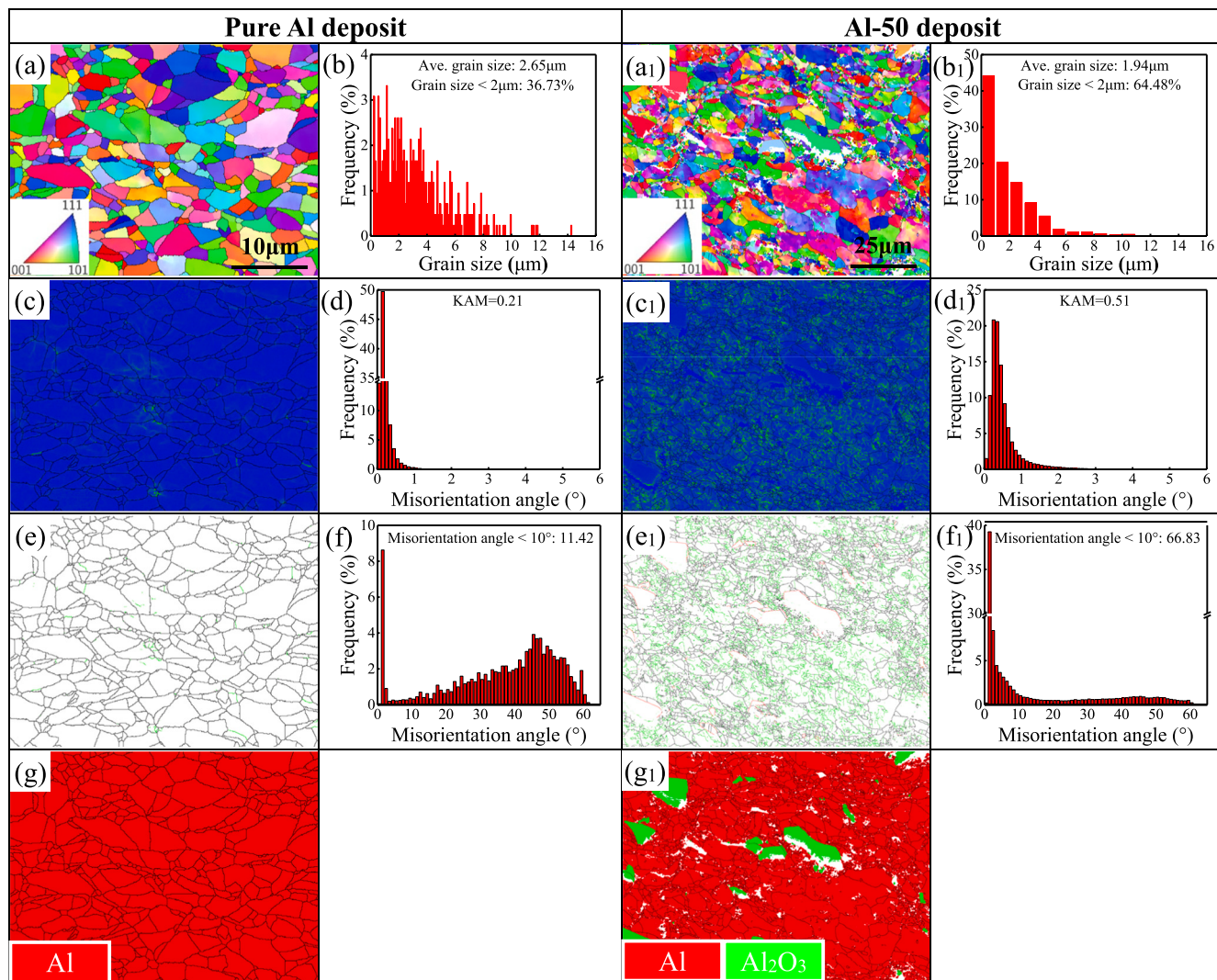


**Fig. 8.** EBSD characterization of CS-AM Al-0 and Al-50 deposit under HT550 conditions, (a) and (a<sub>1</sub>) are inverse pole figure (IPF), (b) and (b<sub>1</sub>) are grain size distribution, (c) and (c<sub>1</sub>) are kernel average misorientation (KAM) map, (d) and (d<sub>1</sub>) are KAM map local misorientation bar, (e) and (e<sub>1</sub>) are grain boundary distribution map, (f) and (f<sub>1</sub>) are corresponding misorientation distribution plot shows the statistic of grain boundaries, (g) and (g<sub>1</sub>) are phase distribution map.

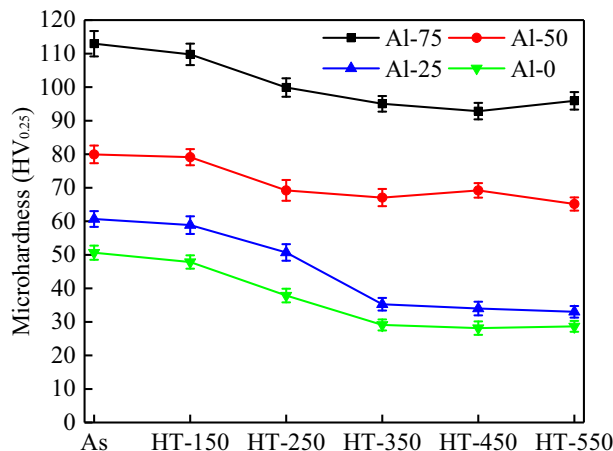
with the grains inside the as-sprayed deposit. This indicates that the grain refinement produced by DRX at this stage still exists. From Fig. 6e & f and e<sub>1</sub> & f<sub>1</sub>, the distribution and density of KAM and LAGBs inside the deposits had slight drop, compared with as-sprayed deposit. It shows that the deposits only recovered after heat treatment.

Fig. 7 shows the EBSD analysis results of Al-0 and Al-50 deposits after heat treatment at 350 °C. From the IPF map (Fig. 7a & a<sub>1</sub>), the morphology of the grains inside the deposits changed significantly, and the elongated oval grains have disappeared and been replaced by new equiaxed grains. The statistical results revealed that the average grain sizes of Al-0 and Al-50 are 2.59 μm and 1.78 μm, respectively, as shown in Fig. 7(b) and Fig. 7(b<sub>1</sub>). This is due to the recovery of grains and static recrystallization (SRX) at this stage [29–31]. The distortion structure inside the deposits re-nucleated and grew during this process [32]. The grain distortion in the Al-50 deposit is more severe, so during the recrystallization process, there are more areas that can form nuclei, resulting in the smaller recrystallized grain size of the Al-50 deposit compared with the Al-0 deposit at this heat treatment temperature. From Fig. 7c & d and c<sub>1</sub> & d<sub>1</sub> that the KAM density of the deposits has reduced. For Al-0 deposit, the proportion of LAGBs is reduced to 44.62% (from Fig. 7e & f), indicating that more LAGBs were converted to HAGBs [29,33,34]. While in Al-50 deposit, the proportion of LAGBs is 67.08%

(from Fig. 7e<sub>1</sub> & f<sub>1</sub>). This indicates that the Al-0 deposit has a higher degree of recrystallization.

Fig. 8 shows the EBSD analysis results of Al-0 and Al-50 deposits after heat treatment at 550 °C. Compared with the sample heat-treated at 350 °C, the grain distribution inside the deposit is more uniform. The statistical results revealed that the average grain sizes of Al-0 and Al-50 are 2.65 μm and 1.94 μm, respectively, and the grain size grows slightly, as shown in Fig. 8(b) and Fig. 8(b<sub>1</sub>). From the KAM map (Fig. 8c), the average grain orientation difference within the Al-0 deposit almost disappeared, indicating that the residual stress in the deposits was almost eliminated. Only few LAGBs have been left in the deposits (Fig. 8e), and the proportion is 11.42% according to Fig. 8f. The ratio of KAM to LAGBS in the Al-50 deposit is still relatively large, which proves that the distortion has not been completely eliminated under this heat treatment condition.

Based on the above discussion, at the lower heat-treatment temperature of 150 °C, the recovery process dominated the microstructural evolution. With increasing the heat-treatment temperature to 350 °C, the recrystallization played an important role to greatly reduce the internal strain. Up to the higher heat-treatment temperature to 550 °C, the grain growth dominated the evolution process [35].



**Fig. 9.** Microhardness of four deposits at different heat treatment temperatures.

### 3.2. Mechanical properties

#### 3.2.1. Microhardness

Hardness is one of the important indicators reflecting the influence of heat treatment. As shown in Fig. 9, the hardness of as-sprayed deposits increased as expected with the addition of hard ceramic particles, owing to the reason that Al<sub>2</sub>O<sub>3</sub> played a role of second-phase strengthening to improve the overall hardness of the deposits. In addition, the hammering effect of Al<sub>2</sub>O<sub>3</sub> particles on Al particles can improve the degree of work hardening of Al particles, thus also can improve the hardness of the deposits. With heat treatment, the hardness evolution of pure Al and composite deposits has a similar trend that a slight decrease occurred at a low temperature (150 °C) annealing stage, and then experienced a sharp drop at 350 °C, followed by a plateau stage.

During the heat treatment at 250 °C, the microstructure of deposits only recovered, and the distortion and dislocations in the microstructure were not eliminated, so the decrease of hardness was small. When heat treated at 350 °C, recrystallization occurred in the deposits, and the distortion and dislocations were eliminated, so the hardness significantly decreased. As the heat treatment temperature continued to increase, the recrystallized grains began to grow, but through the EBSD grain size analysis, the grain growth was not obvious, so the hardness of the deposits did not change significantly.

#### 3.2.2. Tensile properties

Fig. 10a shows the analytical data of ultimate tensile strength (UTS) of CS-AM deposits at different heat treatment temperatures. The UTS of

as-sprayed CS-AM pure Al deposit is 93.3±3.5 MPa. With the addition of Al<sub>2</sub>O<sub>3</sub> particles, the UTS of as-sprayed Al-25 deposits were slightly enhanced to 102.5±2.6 MPa, while the UTS of Al-50 and Al-75 deposits were improved to 119.9±3.7 MPa and 134.1±4.6 MPa, respectively. With the increase of Al<sub>2</sub>O<sub>3</sub> content in the mixed powder, the hammering effect of ceramic particles on the deposited Al becomes more and more intense, which promotes the serious plastic deformation of Al particles and enhances the mechanical interlocking between adjacent particles, resulting in the increase of the UTS of the deposit [8,22,36,37]. After heat treatment at 150 °C, the UTS values of all CS-AM deposits decreased. As the heat treatment temperature raised to 250 °C, the UTS values of all CS-AM deposits had no obvious change. When heat-treated at 350 °C, for pure Al and Al-25 deposits, the abrupt drop of UTS occurred. In comparison, in case of Al-50 and Al-75 deposits, the UTS slightly dropped. With further increase of heat-treatment temperature, there is a slight drop of UTS for all CS-AM deposits.

Fig. 10b shows the tensile elongation data of CS-AM deposits at different heat treatment temperatures. It's noted that with the increase of Al<sub>2</sub>O<sub>3</sub> content, the elongation of as-sprayed CS-AM deposits slightly increased, but the average values are relatively small, i.e., below 4%. When the heat treatment temperature was 150 °C, the elongation of all the deposits did not improve significantly. With further increase of heat-treatment temperature, the elongation of pure Al and Al-25 deposits kept rapid increase, while the elongations of Al-50 and Al-75 deposits increased slowly after 350 °C. In order to explain this phenomenon, the fracture morphology of CS-AM deposits was analyzed, as explained in 3.2.3.

#### 3.2.3. Tensile fracture mechanism

Fig. 11 shows the fracture morphology of the four as-sprayed CS-AM deposits. As shown in Fig. 11a, the fracture of pure Al deposit almost occurs at the interface between the deposited particles, showing typical brittle fracture characteristics [38]. Fig. 11b-d show the fracture morphologies of as-sprayed CS-AM Al-25, Al-50, Al-75 deposits. As the content of Al<sub>2</sub>O<sub>3</sub> particles increases, the fracture morphology of the deposits gradually shows the characteristics of ductile fracture, such as tearing ridges and dimples, indicating that the plastic deformation ability of the as-sprayed CS-AM deposits is gradually increasing. Therefore, with the increase of Al<sub>2</sub>O<sub>3</sub> content, the fracture elongation of the as-sprayed CS-AM deposits gradually increase. This is because the mechanical properties of the deposits depend on the mechanical interlocking between the particles. As the content of Al<sub>2</sub>O<sub>3</sub> in the original powder increases, the plastic deformation of the pure Al particles under the hammering action of Al<sub>2</sub>O<sub>3</sub> becomes more severe, and the mechanical interlocking between the particles becomes tighter, which effectively suppresses the crack nucleation in the deposit, so the cohesion strength and fracture elongation of the deposits is greatly improved.

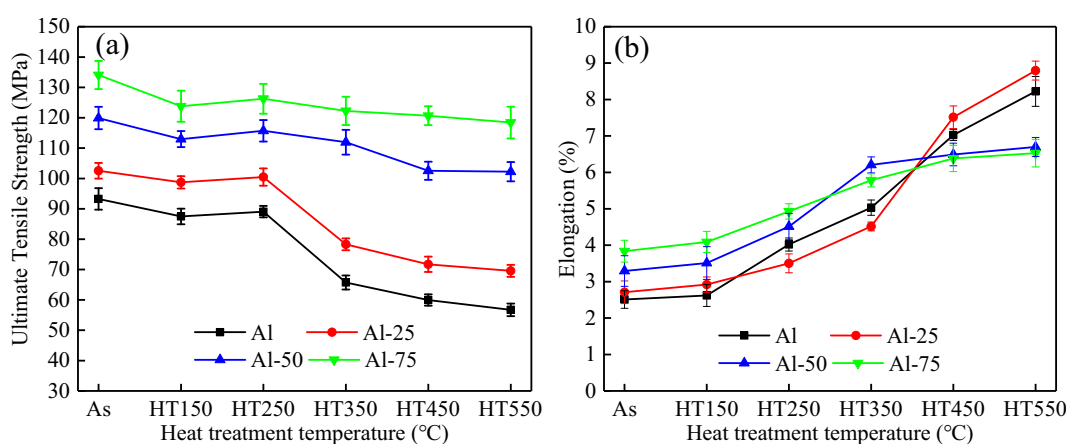


**Fig. 10.** The tensile strength and elongation of CS-AM deposits at different heat treatment temperatures, (a) Ultimate Tensile Strength, (b) Elongation.

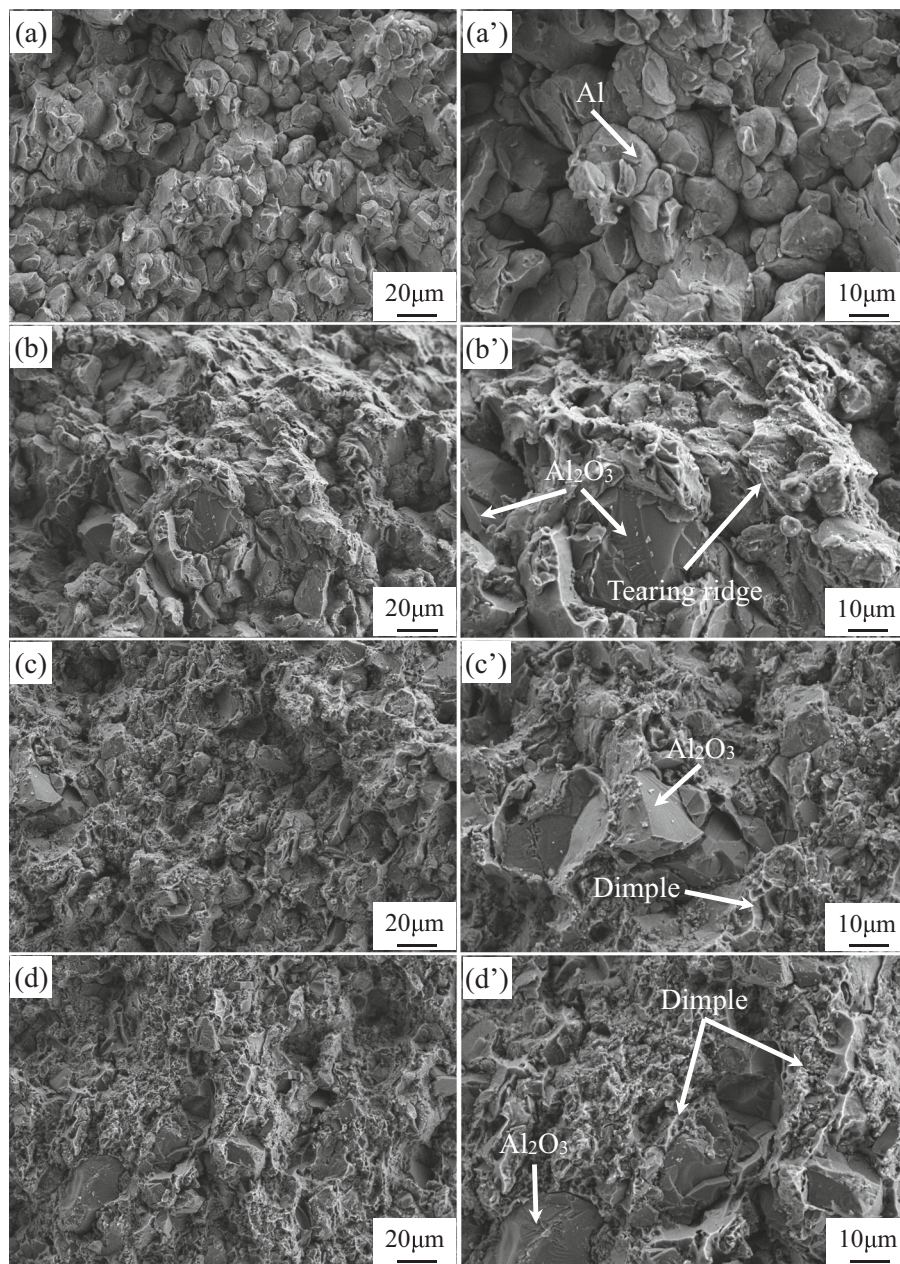


**Fig. 11.** The tensile fracture morphology of CS-AM deposits with different mass fractions of  $\text{Al}_2\text{O}_3$  at as-sprayed state, (a) Al, (b) Al-25, (c) Al-50, (d) Al-75 and (a'), (b'), (c') and (d') are the high-magnification images.

On the other hand, the research by Rokni et al. [39] showed that 99% of the kinetic energy of the deposited particles during the cold spraying process is converted into plastic deformation dissipation energy, which is mainly converted into internal energy. Specifically, the temperature of the impact area increased sharply. When hard  $\text{Al}_2\text{O}_3$  particles are deposited, plastic deformation cannot occur, and the kinetic energy is mainly converted into the plastic dissipation energy of pure Al particles. Therefore, the temperature of Al particles in the composite powder increases more drastically during the deposition process, and it is easier to achieve metallurgical bonding between adjacent Al particles. Therefore, the addition of  $\text{Al}_2\text{O}_3$  particles is beneficial to improve the ductility and UTS of the as-sprayed CS-AM deposits.

Fig. 12 shows the fracture morphology of the heat-treated deposits. When the heat treatment temperature is 150 °C, the fracture morphology of all heat-treated deposits does not change significantly compared with the as-sprayed deposits, so the elongation of the deposit

does not improve obviously. But, after heat treatment at 150 °C, the UTS values of all CS-AM deposits decreased. This is due to the fact that in the process of low temperature heat treatment, the deformed Al particles experienced low temperature recovery, and the residual compressive stress formed in the process of cold spraying gradually released.

When the temperature rises to 250 °C, the number of dimples in the fracture morphology of each deposit increases significantly, indicating that the proportion of metallurgical bonding between adjacent particles increases. Moreover, the additional sintering that occurs at particle-particle interface in the course of annealing reduces crack nucleation sites naturally existed in the deposits [39]. As the heat treatment temperature increases, the size of dimples in the fracture morphology gradually increases as well, as shown in Fig. 12c–e, c<sub>1</sub>–e<sub>1</sub>, c<sub>2</sub>–e<sub>2</sub> and c<sub>3</sub>–e<sub>3</sub>, indicating that the ductility of the deposit gradually increases, which is in good agreement with the elongation results in Fig. 10. It can be seen from the EBSD results that when the heat treatment temperature

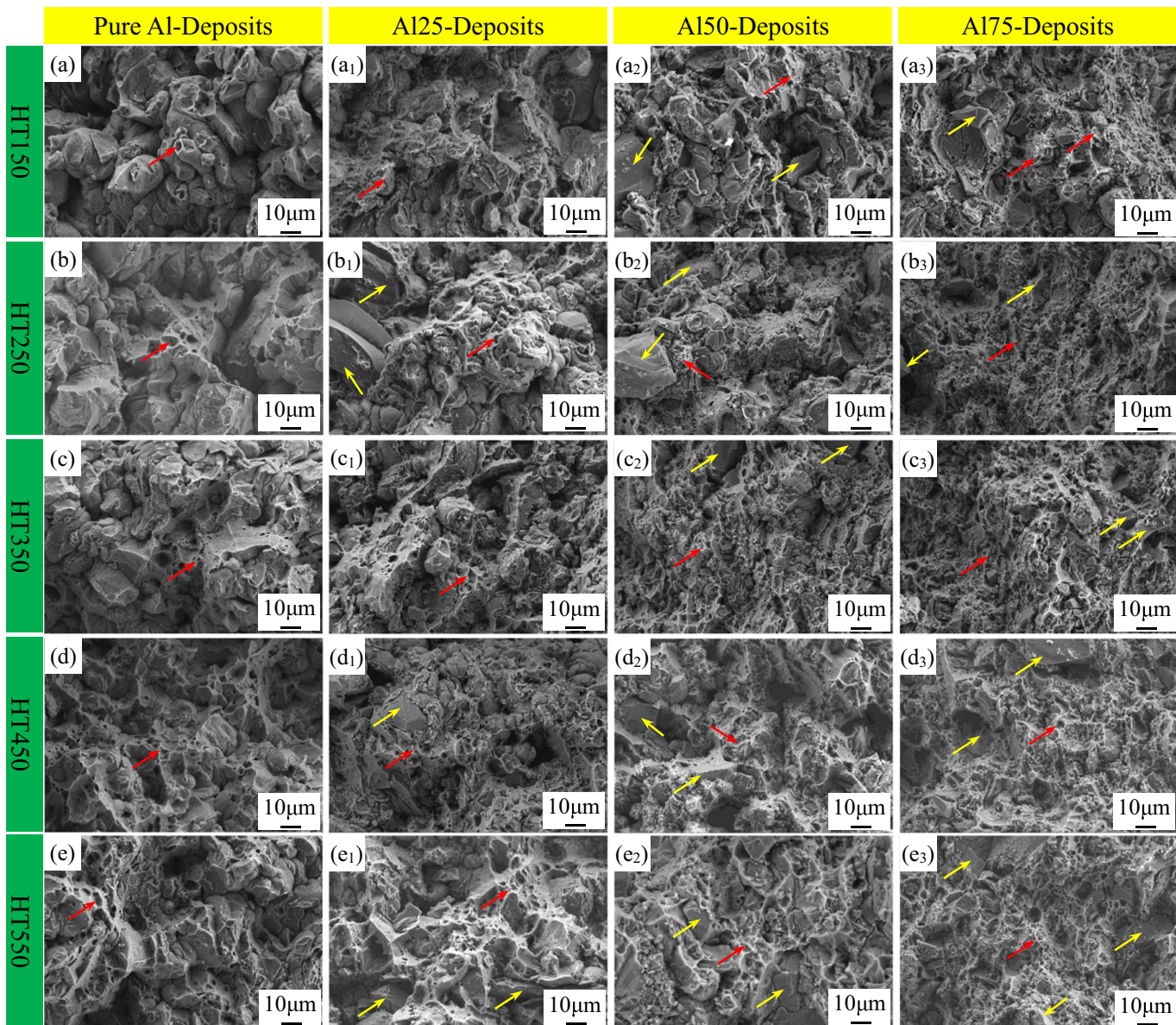


**Fig. 12.** The tensile fracture morphology of CS-AM deposits with different mass fractions of  $\text{Al}_2\text{O}_3$  at different heat treatment temperatures. (a), (b), (c), (d), (e) are pure Al-deposits, (a<sub>1</sub>), (b<sub>1</sub>), (c<sub>1</sub>), (d<sub>1</sub>), (e<sub>1</sub>) are Al25-deposits, (a<sub>2</sub>), (b<sub>2</sub>), (c<sub>2</sub>), (d<sub>2</sub>), (e<sub>2</sub>) are Al50-deposits, (a<sub>3</sub>), (b<sub>3</sub>), (c<sub>3</sub>), (d<sub>3</sub>), (e<sub>3</sub>) are Al75-deposits. In the figure, the yellow arrow indicates  $\text{Al}_2\text{O}_3$ , and the red arrow indicates fracture dimples. (For interpretation of the references to color in this figure legend, the reader is referred to the web version of this article.)

is 350 °C, the deformed Al particles were recrystallized. And as the temperature further increases, the grains gradually grow up, resulting in the decrease of UTS in the temperature range of 250 °C -550 °C. However, in case of Al-50 and Al-75 deposits, owing to the relatively high content of  $\text{Al}_2\text{O}_3$  particles which played the role of second-phase strengthening, the decrease rate of UTS is relatively slow.

#### 4. Conclusion

In the present work, AMCs deposits were prepared by cold spraying, and the effect of  $\text{Al}_2\text{O}_3$  content and heat treatment temperature on the microstructure and mechanical properties was comprehensively studied. The following main conclusions can be drawn from this work:

- (1) The deposits prepared by cold spraying has a dense microstructure and uniform distribution of  $\text{Al}_2\text{O}_3$  particles. As the content of  $\text{Al}_2\text{O}_3$  in the mixed powder increases, hard  $\text{Al}_2\text{O}_3$  particles are

likely to collide with each other during the deposition process, resulting in an increase of the porosity of CS-AM deposits.

- (2) With the increase of  $\text{Al}_2\text{O}_3$  content, the hardness of the deposits gradually increases, and the hammering effect of hard particles on deposited Al particles during the deposition process becomes more and more intense, which effectively improves the interface bonding between Al particles and increases the UTS and deformation ability of the deposits.
- (3) When the heat treatment temperature is in the range of 150 °C-250 °C, the grain distortion and residual compressive stress caused by severe plastic deformation gradually disappear through recovery process. Owing to the recrystallization and grain growth at high heat treatment temperatures of 350 °C-550 °C, the UTS of Al-0 and Al-25 deposits experiences a sharp drop, while the second-phase strengthening of high  $\text{Al}_2\text{O}_3$  content in Al-50 and Al-75 deposits slows the decrease of UTS.

- (4) As the heat treatment temperature increases, the bonding mechanism between adjacent Al particles gradually changes from mechanical interlocking to metallurgical bonding, resulting in a significant improvement of the ductility of CS-AM deposits.

### CRediT authorship contribution statement

**Qiang Wang:** Conceptualization, Methodology, Writing-original draft, Supervision, Project administration, Funding acquisition. **Xu Li:** Methodology, Validation, Finite element numerical simulation, Formal analysis, Investigation, Writing-review & editing. **Ju Yang:** Validation, Formal analysis, Resources, Data curation. **Wenjuan Niu:** Software, Validation, Formal analysis, Data curation, Funding acquisition. **Le Zhai:** Assist in laser shock peening experiment. **Ming-Xing Zhang:** Theoretical guidance. **Peng Han:** Validation, Formal analysis.

### Declaration of competing interest

The authors declare that they have no known competing financial interests or personal relationships that could have appeared to influence the work reported in this paper.

### Acknowledgements

The authors are grateful for the funding support from Shaanxi Key Laboratory of Surface Engineering and Remanufacturing (tywl2019-02), Xi'an University.

### References

- [1] C.W. Ziemian, M.M. Sharma, B.D. Bouffard, T. Nissley, T.J. Eden, in: Materials & Design (1980-2015) 54, 2014, pp. 212–221.
- [2] C. Wang, Y. Chen, T. Li, B. Yao, Appl. Surf. Sci. 256 (2009) 1609–1613.
- [3] W. Zhang, C. Yan, K. Du, F. Wang, Electrochim. Acta 55.2 (2009) 560–571.
- [4] W.X. Zhang, Z.H. Jiang, G.Y. Li, Q. Jiang, J.S. Lian, Appl. Surf. Sci. 254 (2008) 4949–4955.
- [5] R.G. Maev, S.A. Titov, V. Leshchynsky, D. Dzhurinskiy, M. Lubrick, J. Therm. Spray Technol. 20 (2011) 845–851.
- [6] D.V. Dudina, I.S. Batraev, V.Y. Ulianitsky, M.A. Korchagin, Ceram. Int. 40 (2014) 3253–3260.
- [7] D.V. Dudina, G.A. Pribytkov, M.G. Krinitcyn, M.A. Korchagin, N.V. Bulina, B. Bokhonov, I.S. Batraev, D.K. Rybin, V.Y. Ulianitsky, Ceram. Int. 42 (2016) 690–696.
- [8] J. Xu, B. Zou, S. Tao, M. Zhang, X. Cao, J. Alloys Compd. 672 (2016) 251–259.
- [9] M.R. Rokni, C.A. Widener, G.A. Crawford, M.K. West, Mater. Sci. Eng. A 625 (2015) 19–27.
- [10] A. Kurt, I. Uygur, E. Cete, J. Mater. Process. Technol. 211 (2011) 313–317.
- [11] A.M. Vilardell, N. Cinca, A. Concstell, S. Dosta, I.G. Cano, J.M. Guilemany, J. Mater. Sci. 50 (2015) 4441–4462.
- [12] A. Concstell, J.J.P. Henao, S. Dosta, N. Cinca, I.G. Cano, J.M. Guilemany, J. Alloys Compd. 651 (2015) 764–772.
- [13] V. Stathopoulos, V. Sadykov, S. Pavlova, Y. Bespalko, Y. Fedorova, L. Bobrova, A. Salanov, A. Ishchenko, V. Stoyanovsky, T. Larina, V. Ulianitsky, Z. Vinokurov, V. Kriventsov, Surf. Coat. Technol. 295 (2016) 20–28.
- [14] H. Miura, S. Isa, K. Omuro, J. Non-Cryst. Solids 61–62 (1984) 163–168.
- [15] N. Yuvaraj, S. Aravindan, Vipin 4 (2015) 398–410.
- [16] A. Chaudhuri, Y. Raghupathy, D. Srinivasan, S. Suwas, C. Srivastava, Acta Mater. 129 (2017) 11–25.
- [17] K. Spencer, D.M. Fabijanic, M.X. Zhang, Surf. Coat. Technol. 206 (2012) 3275–3282.
- [18] Q. Wang, K. Spencer, N. Birbilis, M.-X. Zhang, Surf. Coat. Technol. 205 (2010) 50–56.
- [19] W.Y. Li, N. Li, X.W. Yang, Y. Feng, A. Vairis, Mater. Sci. Eng. A 702 (2017) 73–80.
- [20] A. Rahbar-kelishami, A. Abdollah-zadeh, M.M. Hadavi, R.A. Seraj, A.P. Gerlich, Appl. Surf. Sci. 316 (2014) 501–507.
- [21] Y.L. Liang, Z.B. Wang, J. Zhang, J.B. Zhang, K. Lu, Appl. Surf. Sci. 385 (2016) 341–348.
- [22] C. Huang, W. Li, Z. Zhang, M. Fu, M.-P. Planche, H. Liao, G. Montavon, Surf. Coat. Technol. 296 (2016) 69–75.
- [23] P. Babu, D. Lahiri, I. Ganesh, A. Agarwal, J. Therm. Spray Technol. 23 (2013).
- [24] R. Messer, S. Dais, D. Wolf, Proc 18th Ampère Congress. Nottingham, 1974.
- [25] K. Spencer, V. Luzin, N. Matthews, M.X. Zhang, Surf. Coat. Technol. 206 (2012) 4249–4255.
- [26] Q. Wang, N. Birbilis, M.-X. Zhang, Mater. Lett. 65 (2011) 1576–1578.
- [27] Y. Zou, W. Qin, E. Irisso, J.-G. Legoux, S. Yue, J.A. Szpunar, Scr. Mater. 61 (2009) 899–902.
- [28] A. Tripathi, S. Zaeferer, Ultramicroscopy 207 (2019), 112828.
- [29] T. Liu, W.A. Story, L.N. Brewer, Metall. Mater. Trans. A Phys. Metall. Mater. Sci. 50 (2019) 3373–3387.
- [30] K.S. Al-Hamdan, J.W. Murray, T. Hussain, A.T. Clare, Surf. Coat. Technol. 374 (2019) 21–31.
- [31] A. Sabard, H.L.D.V. Lovelock, T. Hussain, J. Therm. Spray Technol. 27 (2018) 145–158.
- [32] V. Luzin, K. Spencer, M.X. Zhang, Acta Mater. 59 (2011) 1259–1270.
- [33] Z. Du, S. Xiao, L. Xu, J. Tian, F. Kong, Y. Chen, Mater. Des. 55 (2014) 183–190.
- [34] M.R. Rokni, C.A. Widener, V.K. Champagne, G.A. Crawford, S. Nutt, Surf. Coat. Technol. 310 (2017) 278–285.
- [35] R. Huang, M. Sone, W. Ma, H. Fukanuma, Surf. Coat. Technol. 261 (2015) 278–288.
- [36] X. Wang, L. Zhang, X. Zhou, W. Wu, X. Jie, Surf. Coat. Technol. 386 (2020), 125486.
- [37] K. Spencer, D.M. Fabijanic, M.X. Zhang, Surf. Coat. Technol. 204 (2009) 336–344.
- [38] W. Sun, A. Bhowmik, A.W.Y. Tan, R. Li, F. Xue, I. Marinescu, E. Liu, J. Alloys Compd. 797 (2019) 1268–1279.
- [39] M.R. Rokni, C.A. Widener, V.K. Champagne, G.A. Crawford, S.R. Nutt, Surf. Coat. Technol. 310 (2017) 278–285.